Environmental Science & Technology

pubs.acs.org/est

Article

Initial pH Governs Secondary Organic Aerosol Phase State and Morphology after Uptake of Isoprene Epoxydiols (IEPOX)

Ziying Lei, Yuzhi Chen, Yue Zhang, Madeline E. Cooke, Isabel R. Ledsky, N. Cazimir Armstrong, Nicole E. Olson, Zhenfa Zhang, Avram Gold, Jason D. Surratt,* and Andrew P. Ault*

Cite This: *Environ. Sci. Technol.* 2022, 56, 10596−10607

Read Online

ACCESS | Metrics & More | Article Recommendations | Supporting Information

ABSTRACT: Aerosol acidity increases secondary organic aerosol (SOA) formed from the reactive uptake of isoprene-derived epoxydiols (IEPOX) by enhancing condensed-phase reactions within sulfate-containing submicron particles, leading to low-volatility organic products. However, the link between the initial aerosol acidity and the resulting physicochemical properties of IEPOX-derived SOA remains uncertain. Herein, we show distinct differences in the morphology, phase state, and chemical composition of individual organic−inorganic mixed particles after IEPOX uptake to ammonium sulfate particles with different initial atmospherically relevant acidities (pH = 1, 3, and 5). Physicochemical properties were characterized via atomic force microscopy coupled with photothermal infrared spectroscopy (AFM-PTIR) and Raman microspectroscopy. Compared to less acidic particles (pH 3 and 5), reactive uptake of IEPOX to the most acidic particles (pH 1) resulted in 50% more organosulfate formation, clearer phase separation (core−shell), and more irregularly shaped morphologies, suggesting that the organic phase transitioned to semisolid or solid. This study highlights that initial aerosol acidity may govern the subsequent aerosol physicochemical properties, such as viscosity and morphology, following the multiphase chemical reactions of IEPOX. These results can be used in future studies to improve model parameterizations of SOA formation from IEPOX and its properties, toward the goal of bridging predictions and atmospheric observations.

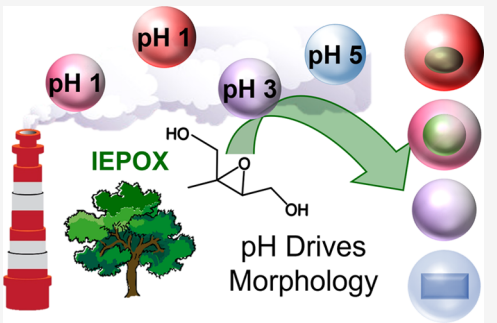

KEYWORDS: *aerosol acidity, multiphase chemistry, organosulfates, isoprene oxidation products, aerosol viscosity*

1. INTRODUCTION

Atmospheric aerosols significantly affect air quality, human health, and climate; particularly submicron particles, which have long atmospheric lifetimes, determine cloud nucleating properties, and penetrate deeply into the lungs after inhalation.[1] Secondary organic aerosol (SOA) is a component of atmospheric aerosols formed by the oxidation of volatile organic compounds (VOCs) followed by nucleation, condensation, or multiphase chemical reactions of the resulting low-volatility oxidation products.[2,3] SOA is ubiquitous, accounting for a large mass fraction of submicron aerosol particles.[4−6] Recent studies have shown that SOA frequently represents a greater fraction of fine particulate matter ($PM_{2.5}$, particles with a diameter <2.5 μm) than primary organic aerosol (POA).[7,8] SOA being more abundant than POA is true globally across both urban and rural settings.[9,10] SOA has recently been shown to be associated with a 6.5× increase in mortality versus overall $PM_{2.5}$.[11] Recent studies have shown that SOA is possibly linked to adverse human health outcomes upon inhalation exposure, including early biological changes within lung cells that are associated with inflammation and oxidative stress.[12−16]

Isoprene has the highest emissions of any nonmethane VOC with global emission rates of ∼500 Tg/y[17,18] and undergoes oxidation to form lower volatility gaseous species, such as isoprene epoxydiols (IEPOX).[19,20] When the oxidation of isoprene to IEPOX occurs, the increasing molecular functionality and decreasing vapor pressure (3×10^{-6} atm)[21] facilitate reactive uptake to existing aerosol particles,[3,7,22−24] particularly under low pH conditions when the epoxide can be opened via acid-driven reaction pathways.[25,26] Previous studies have shown that high IEPOX reactive uptake to inorganic sulfate particles leads to the formation of substantial amounts of aerosol mass, especially in the Southeastern United States.[27−30] Due to the large mass loadings of IEPOX-derived SOA, which can contribute up to 40% of the submicron organic aerosol mass in isoprene-rich environments,[27,31] the physicochemical properties (i.e., phase state and morphology) of these aerosol particle types can affect further SOA formation and the evolution of existing SOA.[32−34]

Received: March 4, 2022
Revised: June 25, 2022
Accepted: June 28, 2022
Published: July 14, 2022

Table 1. Solutions Used for Seed Aerosol, Labels Used in Text, Measured Solution pH with Uncertainty Prior to Aerosolization, and Concentrations of Sulfuric Acid and Ammonium Sulfate[a]

seed acidic aerosol solution	label	measured pH	$[H_2SO_4]$	$[(NH_4)_2(SO_4)]$
pH = 1 without ammonium	pH 1 w/o NH_4^+	1.05 ± 0.01	0.12 M	N/A
pH = 1 with ammonium	pH 1 w/NH_4^+	1.32 ± 0.01	0.06 M	0.06 M
pH = 3	pH 3	2.99 ± 0.01	0.0025 M	0.1175 M
pH = 5	pH 5	5.19 ± 0.01	N/A	0.12 M

[a]N/A = not applicable.

The phase state (liquid, semisolid, or solid) of atmospheric particles plays a critical role in determining their ability for further chemical reactions in the aerosol phase.[33,35−37] In the past decade, studies have shown that SOA particles can exist in an amorphous semisolid or solid state under different ambient conditions (e.g., relative humidity (RH) and temperature)[38,39] and the viscosity of SOA particles can have a wide range of viscosities from 3×10^1 Pa s (similar to honey) to 3.7×10^8 Pa s (similar to tar pitch).[38,40−43] Multiphase chemistry of IEPOX leads to the formation of organosulfates,[44−47] polyols,[7,48−51] and oligomers[3,52,53] in the condensed phase, whose increased molecular weights result in more viscous aerosol (i.e., 10^6 Pa s).[54] Previous studies have shown that increased viscosity leads to longer mixing timescales for molecules within particles, which decreases subsequent gaseous IEPOX uptake and SOA formation.[33,54−56] Due to decreased miscibility of organic components in high ionic strength aqueous phases, the viscous organic components of a particle salt out to form an outer layer (i.e., shell) at the edge of the inorganic components (i.e., core), commonly referred to as core−shell morphology.[57−59] For the resulting core−shell morphology, if the shell is highly viscous, it can kinetically inhibit further uptake of gaseous species,[42,60] reactivity,[34,54,61,62] and ultimately SOA growth and evolution in the atmosphere.[42] Thus, understanding the phase state, viscosity, and morphology of SOA particles is central to predicting heterogeneous uptake of IEPOX leading to SOA formation.

Aerosol pH also has substantial impacts on SOA formation by modifying the reaction rates of organic species within the condensed phase.[63,64] Many atmospheric multiphase chemical processes are pH-dependent, including the reactive uptake of IEPOX to form SOA and many subsequent reactions in the condensed phase.[23,24,65] Atmospheric chamber experiments have observed that greater SOA formation occurs under acidic conditions (pH 1.5) compared to neutral conditions (pH 5).[49,66] As an example, the acid-driven ring-opening reaction of IEPOX leads to lifetimes of <1 min after uptake to particles with pH <1, but IEPOX can have lifetimes of hours to days in particles at pH 5 under typical atmospheric conditions.[2,23] It is also important to consider the role of ammonia/ammonium in impacting SOA formation as ammonia is the most important atmospheric base[67,68] and impacts aerosol pH.[69,70] There remains considerable uncertainty regarding how aerosol pH impacts the resulting morphology and viscosity after IEPOX uptake.

Further experimental data are needed to improve our current understanding of how exactly acid-catalyzed multiphase chemical reactions of gaseous IEPOX with particles of varying acidity subsequently affect particle morphology and viscosity. In this study, we investigated changes in particle phase state and morphology after gaseous IEPOX uptake onto particles generated from mixtures of ammonium sulfate and sulfuric acid with a range of initial acidities (pH = 1, 3, and 5). The time-resolved modification of particle morphology and chemical composition after different reaction times (i.e., 30, 60, and 120 min after gaseous IEPOX injection) were also characterized. Individual particles were characterized using multiple microspectroscopy methods (atomic force microscopy coupled with photothermal infrared (AFM-PTIR) spectroscopy, Raman microspectroscopy, and scanning electron microscopy (SEM)) to provide detailed information on individual particle morphology, phase state, and chemical composition during and after IEPOX reactive uptake. These single-particle data were compared with changes in aerosol size distributions and organosulfate concentrations of the total aerosol generated during our chamber studies. Establishing the physicochemical properties of SOA formed under varying initial pH conditions is important for improved model representation of SOA and, more broadly, for resolving the impacts of atmospheric aerosol on human health and climate.[71−73]

2. METHODS

2.1. Chamber Experiments. Aerosol particles were generated from solutions with different pH values where the concentration of the inorganic sulfate ions (sulfate ($[SO_4^{2-}]$) + bisulfate ($[HSO_4^-]$)) was kept at 0.12 M for each solution. Solutions were prepared using ammonium sulfate (Sigma-Aldrich, ≥99% purity), sulfuric acid (Sigma-Aldrich, ≥98% purity), and 18.2 MΩ Milli-Q water (Table 1), without further purification. The pH, chemical composition, and submicron size of the seed aerosol were chosen to represent conditions under which SOA formation reactions occur in the atmosphere.[74−76]

The pH of the bulk solutions was measured by a pH probe (PHS-3C, Yantai Stark Instrument Co.). Aerosols were generated from a constant output atomizer (TSI Inc., Model 3076) and then passed through diffusion driers to reach 50% RH, which is above the efflorescence RH of ammonium sulfate and sulfuric acid to maintain the aerosol in an aqueous phase state. The number size distribution of the different seed aerosols (mode diameters: 83−103 nm) and SOA aerosols after reacting with IEPOX for 120 min (101−133 nm) are shown in Figure S1. Acidic seed particles were injected into the 10-m^3 indoor chamber at the University of North Carolina at Chapel Hill (UNC) chamber facility that was prehumidified to 50% RH,[34,49] and the concentration was allowed to stabilize for 30 min. Synthesized *trans*-β-IEPOX,[77] which is the predominant IEPOX isomer in the atmosphere,[20] was dissolved in ethyl acetate and gaseous IEPOX was injected into the chamber using a high-purity nitrogen flow of 2 L min^{-1} for 10 min and then 4 L min^{-1} for 50 min through a heated manifold (60 °C).[24,33,34,49,55] The seed particles with different initial pH values reacted with gaseous IEPOX to form IEPOX-derived SOA. A scanning electrical mobility spectrometer (SEMS, BMI Inc., Model 2100) was used to monitor the particle growth by

https://doi.org/10.1021/acs.est.2c01579
Environ. Sci. Technol. 2022, 56, 10596−10607

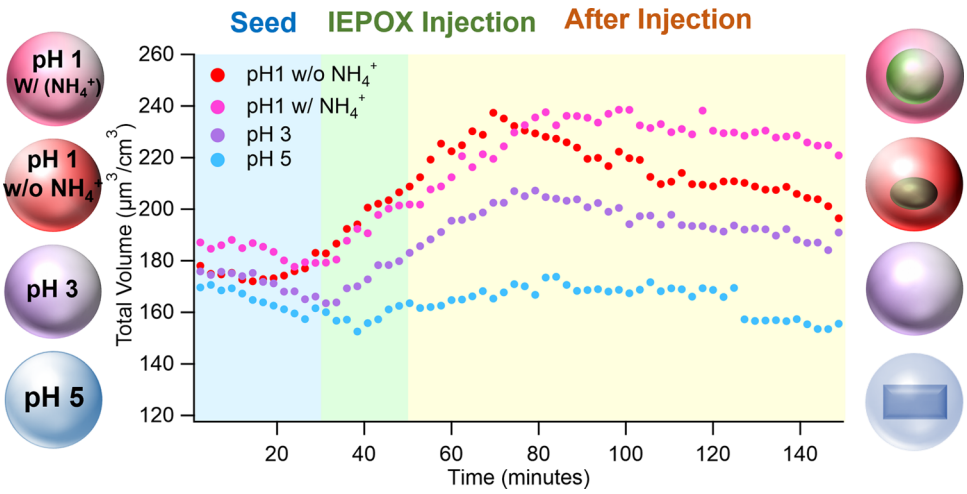

Figure 1. Particle volume concentration ($\mu m^3/cm^3$) after IEPOX uptake for different acidic inorganic sulfate particles: pH 1 (NH_4^+, HSO_4^- ≫ SO_4^-, H^+, H_2O) (pink solid circle), pH 1 (HSO_4^-, H^+, H_2O) (red solid circle), pH 3 (NH_4^+, H^+, SO_4^{2-} ≫ HSO_4^-, H_2O) (purple solid circle), and pH 5 (NH_4^+, H^+, SO_4^{2-}, H_2O) (blue solid circle). The volume concentration is calculated from integrated size distributions and has not been corrected for particle wall loss.

measuring aerosol size distributions, number concentrations (#/cm^3), and volume concentrations ($\mu m^3/cm^3$) in the chamber. After the seed particles were exposed to the injected IEPOX for 30, 60, and 120 min, aerosol particles were inertially impacted onto substrates for microscopy using an eight-stage mini-multi orifice uniform deposit impactor (mini-MOUDI, Model 135, TSI Corp.). Particles were analyzed from stage 7, which has a 50% aerodynamic cut point of 320 nm (d_{50}) leading to particles with diameters of 180−320 nm on the substrates. Microscopy substrates included silicon wafers (16014, Ted Pella, Inc.), carbon-type-b Formvar-coated copper transmission electron microscopy (TEM) grids (1GC50, Ted Pella, Inc.), and quartz pieces (26016, Ted Pella, Inc.).

2.2. Microscopy Imaging and Spectroscopy. The morphology and phase of individual submicron particles were analyzed using an AFM-PTIR (nanoIR2, Anasys Instruments, Santa Barbara, CA). Particles on silicon substrates were imaged in 5 × 5 μm^2 and 10 × 10 μm^2 regions with 0.7 Hz scan rates that operated at a 0.07−0.4 N/m spring constant and 13 ± 4 kHz resonant frequency. Tapping IR mode was conducted with a gold-coated microfabricated silicon probe (AU.1000.SWTSG, Platypus Technologies). Raw data were processed using SPIP 6.2.6 software (Image Metrology, Hørsholm, Denmark) to measure single-particle height, radius, and volume. The spreading ratios of individual particles were calculated using particle radius divided by particle height (SR = r/h),[32,55,78] as more viscous particles will remain taller on the substrate by spreading less compared to more liquid-like particles with lower viscosity that will spread more. Spreading ratio uncertainties are reported as 2σ of a Gaussian fit to the histogram of spreading ratios. T-tests were used to compare the spreading ratio of seed particles with mixed seed-SOA particles at discrete time points during the experiment (i.e., 30, 60, and 90 min) and were considered to be statistically different for p values <0.05. SEM images were also obtained for particles impacted onto TEM grids using an FEI Helios 650 Nanolab-Dualbeam electron microscope equipped with a high-angle annular dark-field (HAADF) detector operated at an accelerating voltage of 10.0 kV, a current of 0.80 nA, and pressures ranging from 10^{-5} to 10^{-6} Pa.[79]

AFM-PTIR (nanoIR2 system, Anasys Instruments, Santa Barbara, CA) was used to characterize the chemical composition of individual particles. IR spectra were collected using an optical parametric oscillator (OPO) source with a range of 800−3600 cm^{-1} and an average spectral resolution of 2 cm^{-1}. For each sample, the IR spectra were collected at a scan rate of 100 cm^{-1}/s for 5 min acquisitions and averaged after three accumulations.[78]

Raman microspectroscopy was used to characterize the chemical composition of phase-separated particles, as in prior studies.[80] Spectra for both the particle core and shell were collected using a LabRAM HR Evolution Raman micro-spectrometer (Horiba, Ltd.) equipped with a 50 mW 532 nm Nd:YAG laser source, a confocal optical microscope (Olympus, 100 × 0.9 N.A. objective), and a CCD detector. Each Raman spectrum was collected in the range of 500−4000 cm^{-1} with three accumulations at 60 s acquisition times. A diffraction grating with 1800 groove/mm was used to yield a spectral resolution of 0.7 cm^{-1}. Both PTIR and Raman spectra were collected at room temperature, RH, and ambient pressure.

2.3. Characterization of Organosulfate Formation. For each chamber experiment, particles were collected using a particle-into-liquid sampler (PILS, BMI model 4001). PILS samples were collected every 6 min with an air sampling rate of ~6.5 L min^{-1}, resulting in a liquid sample volume of ~1.2 mL, which was used for offline chemical analysis by ion chromatography (IC).[34] IC conditions have been previously summarized by Riva et al.[34,81] PILS samples were stored in the dark at 2 °C immediately after collection and were analyzed within 24 h, as validated in prior work.[34] In this study, the sulfate concentration in the initial atomizer solution was kept constant at 0.12 M (Table 1) and the total particulate organosulfate concentrations with specific reaction time can be calculated by subtracting inorganic sulfate concentrations from the initial sulfate concentration measured by IC (which is initially all inorganic sulfate).[34,82] The initial sulfate concentration of a seed aerosol-only experiment was also analyzed (Figure S2) to compare with IEPOX-derived SOA experiments.

https://doi.org/10.1021/acs.est.2c01579
Environ. Sci. Technol. 2022, 56, 10596−10607

$$[\text{Sulfate}_{\text{Organic}}]_t = [\text{Sulfate}_{\text{Total}}]_0 - [\text{Sulfate}_{\text{IC}}]_t$$

Additionally, 2-methyltetrols (2-MT) and their OS derivative (2-methyltetrol sulfate, 2-MTS) were characterized by hydrophilic interaction liquid chromatography (HILIC)/ESI-HR-quadrupole time-of-flight mass spectrometry (QTOFMS).[34,83]

3. RESULTS AND DISCUSSION

3.1. IEPOX-Derived SOA Formation under Varying Initial Aerosol pH Values. The relative fraction of the HSO_4^- and SO_4^{2-} ions varies as a function of pH (Figure S3), highlighting that bisulfate dominates (>90%) at pH 1 and sulfate dominates at pH 3 (>90%) and pH 5 (>99%) for the initial seed aerosol particles. After gaseous IEPOX was injected into the chamber, the volume concentration ($\mu m^3/cm^3$) of the aerosol increased, with the greatest volume growth observed with pH 1 seed aerosol particles either with or without ammonium (NH_4^+). The total aerosol particle volume reached its maximum value 30−60 min after the IEPOX injection finished (Figure 1). For less acidic seed particles, such as pH 3, the increase in volume concentration was observed after IEPOX uptake, but it is less than the particle volume growth under acidic conditions. A slight increase in total volume occurred for pH 5 particles throughout the experiment and the slight decrease later on during the experiment is due to wall loss after IEPOX is no longer being injected. These results expand on prior studies,[2,65] which only examined acidic versus nonacidic seed particles, and we show here that high $[H^+]$ is needed for growth, with or without ammonium in the seed.

3.2. Phase and Viscosity Evolution during Reactive Uptake of IEPOX. To determine how quickly core−shell morphology formed, AFM phase images were collected after pH 1 seed particles (without NH_4^+ counter ion) were exposed to gaseous IEPOX (Figure 2a). Particles exhibited phase separation after exposure to IEPOX for 30-, 60-, and 120-min reaction times. AFM phase images show that a coating (black color) formed quickly after the initially homogeneous seed aerosol particle is exposed to IEPOX for 30 min, and the circular morphology indicates that the particles were liquid and had not effloresced prior to injection into the chamber.[84−86] With increasing IEPOX:SO_4^{2-} ratios throughout the reaction time (as SO_4^{2-} is incorporated into organosulfates, Figure S4),[34] a thicker coating formed, consistent with the previous studies.[33,34,54] After 60 min of IEPOX uptake, the particle core became smaller and a thicker coating was observed (Figure 2b). After 120 min of IEPOX uptake, the morphology of the core had inclusions, which may suggest the continuous reactive uptake of gaseous IEPOX continued to modify the core, even with a thicker coating, leading to less spherical, aqueous morphology. To further understand the viscosity change during IEPOX uptake, particle spreading ratios were calculated for individual particles.

Particle spreading ratios have been used as an indirect measurement of particle viscosity,[32,55] as more viscous particles spread less on the substrate leading to a smaller spreading ratio. The spreading ratios of pH 1 seed particles (without NH_4^+) and reacted pH 1 seed particles exposed to IEPOX for 30, 60, and 120 min were calculated, and are shown in Figure 2c. The pH 1 seed particles (without NH_4^+) before reaction with IEPOX had an average spreading ratio of 2.8 ± 0.2. Following IEPOX uptake, the average spreading ratios significantly decreased to 1.8 ± 0.1 after 30 min, 2.4 ± 0.1 after 60 min, and 2.1 ± 0.1 after 120 min of reaction time.

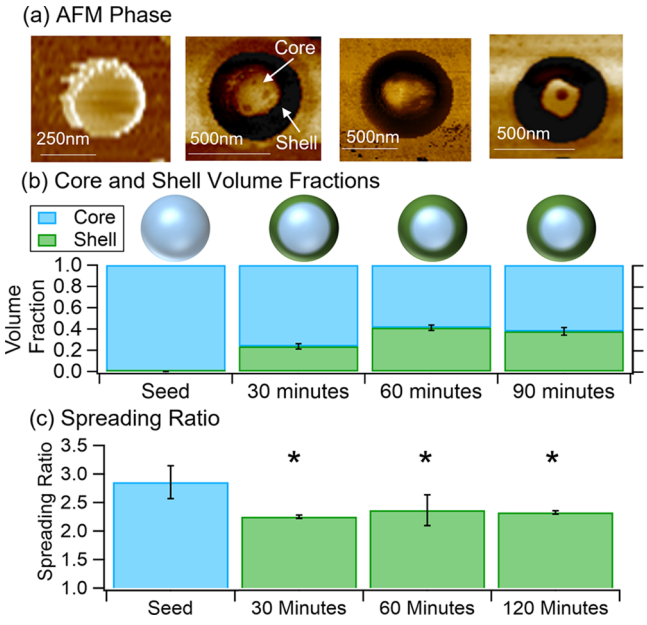

Figure 2. (a) AFM phase image of representative pH 1 w/o NH_4^+ seed particles, particles after reaction with IEPOX for 30, 60, and 120 min; (b) core volume fraction (blue) and shell volume fraction (green), the error bars represent standard error; and (c) averaged spreading ratios of 249, 68, 78, and 74 particles, respectively, single asterisks denote spreading ratios that are statistically different than seed particles before IEPOX uptake ($p < 0.05$), error bars represent 2σ from a Gaussian fit.

Reactive uptake of IEPOX for 30 min led to increased particle viscosity, which has been shown by both measurements by Olson et al.[55] using an entrained-aerosol flow tube reactor with <1 min residence time and modeling results from Zhang et al.[82] The formation of organosulfates and other oligomers has been shown to increase particle viscosity and phase separations.[34,55] After reacting for 60 and 120 min, a thicker coating formed and a smaller core was observed, which suggests that IEPOX was continuously reacting with seed particles, though the spreading ratios did not change significantly. This suggests most viscosity increases are likely facilitated by organosulfate formation that occurs within 60 min, and that the particles were stable for at least the next hour, potentially due to a self-limiting effect.[54] These results demonstrate rapid modification of submicron particle-phase states and viscosity during reactive uptake of gaseous IEPOX to pH 1 seed particles (without NH_4^+).

3.3. Morphology and Phase Modifications after IEPOX Uptake under Varying Aerosol Acidity Conditions. Particle volume concentrations of seed particles and particles after IEPOX uptake for 60 min are shown in Figure 3 (top row). A significant increase in IEPOX-derived SOA formation was observed for pH 1 seed particles with and without NH_4^+, with volume concentrations increasing 34.0 ± 0.4 and 31.9 ± 0.1%, respectively. Similarly, the less acidic seed particles led to less volume growth (13.4 ± 0.9% for pH 3 ammonium sulfate and 17.3 ± 0.3% for pH 5 ammonium sulfate). These results are consistent with previous studies that show IEPOX-derived SOA formation is facilitated by acid-driven particle-phase reactions.[49,54] In addition, average height traces of 10 individual particles are included in Figure 3 (middle row), which shows the average aerosol growth after SOA formation. A taller particle with the same width indicates

https://doi.org/10.1021/acs.est.2c01579
Environ. Sci. Technol. 2022, 56, 10596−10607

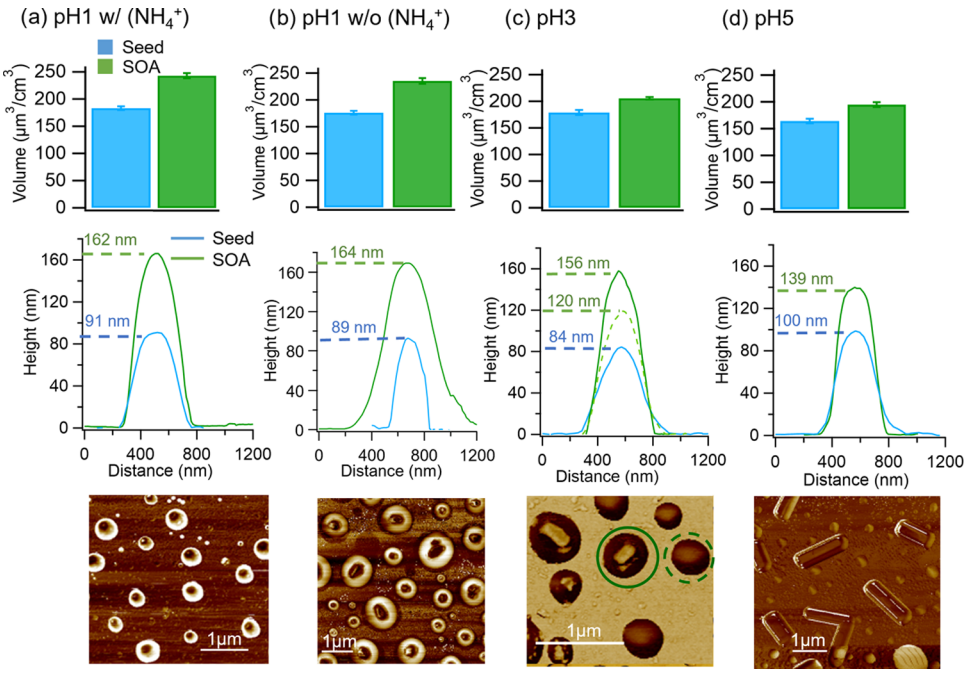

Figure 3. Particle volume concentration (top row), average height trace of 10 individual particles (middle row), and AFM phase images (bottom row) for 60 min reaction. (a) pH 1 seed particles with ammonium after IEPOX uptake; (b) pH 1 seed particles without ammonium after IEPOX; (c) pH 3 seed particles after IEPOX uptake; and (d) pH 5 seed particles after IEPOX uptake. The blue color represents the seed particles, and the green color represents the IEPOX-derived SOA particles. For pH 3, the solid trace represents the SOA particles with a distinct core, and the dashed line represents more liquid-like SOA particles.

a more viscous particle while a shorter particle is less viscous and has spread more.[55] As seed particles became less acidic, the height and, by proxy, the viscosity of particles after IEPOX uptake was lower. This is because IEPOX-derived organosulfates (and oligomers) that increase particle viscosity are more likely to be formed under acidic conditions.[33,34,55,87] To connect greater SOA formation and higher viscosity to core−shell morphology, AFM phase imaging was used to characterize particles after gaseous IEPOX uptake onto particles with different initial pH values. AFM phase images in Figure 3 (bottom row) demonstrate that phase separation only occurs for the pH 1 particles (with or without NH_4^+) after exposure to gaseous IEPOX. AFM phase images suggest that the SOA particles generated under acidic conditions formed a thick SOA coating and the circular core−shell morphology illustrates that those particles are phase separated. For less acidic seed particles (pH 3), the mixture of particles with crystalized and spherical cores shows evidence of less organosulfate formation after IEPOX uptake. For near neutral (pH 5) seed particles, ammonium sulfate crystals are present, which further indicates that minimal organic material has formed (consistent with aerosol volume concentration data), as organic material interferes with crystallization leading to round amorphous solids.[88,89] SEM images were also collected to confirm the phase transition, and the result is consistent with AFM (Figure S5). To understand the chemical composition of the individual core−shell IEPOX-derived SOA particles, PTIR and Raman spectra were collected.

3.4. Chemical Characterization of Core−Shell Morphology Particles. Chemical composition plays an important role in understanding phase-separated inorganic-SOA mixed particles. Raman microspectroscopy and PTIR were used to identify functional group composition for the core and shell of these particles. Detailed spectra of pH 1 seed particles with NH_4^+ after IEPOX uptake for 60 min were collected (Figure 4), and the specific vibrational modes and full Raman spectra are listed in the Supporting Information (Table S1). A strong sulfate peak $\nu_s(SO_4^{2-})$ at 976 cm^{-1} in the Raman spectra is clearly discernible and located in both core and shell of particles and the bisulfate $\nu_s(HSO_4^-)$ peak at 1041 cm^{-1} was also observed.[80,90−92] Both the particle core and shell also showed signs of organosulfate formation with peaks around

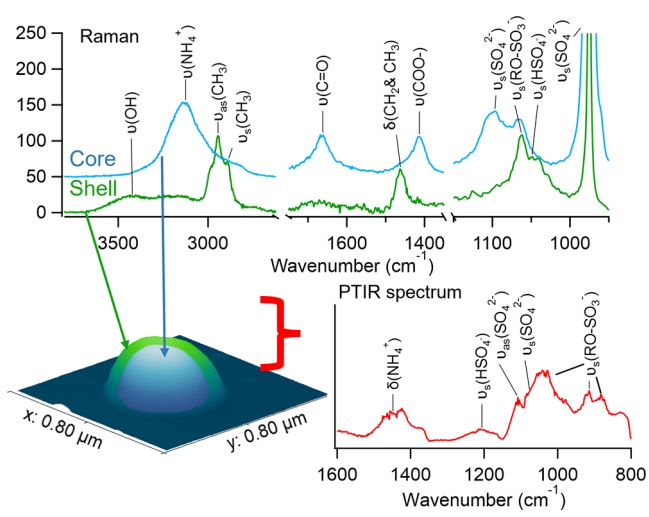

Figure 4. Raman spectra of pH 1 seed particles with NH_4^+ after IEPOX reactive uptake for 60 min, showing the differences between core (blue) and shell (green) composition (top), AFM three-dimensional (3D) image of individual submicron particles after impact on the Si substrate (bottom left); representative PTIR spectra of the whole particle for a different core−shell SOA-inorganic particle formed from IEPOX uptake.

https://doi.org/10.1021/acs.est.2c01579
Environ. Sci. Technol. 2022, 56, 10596−10607

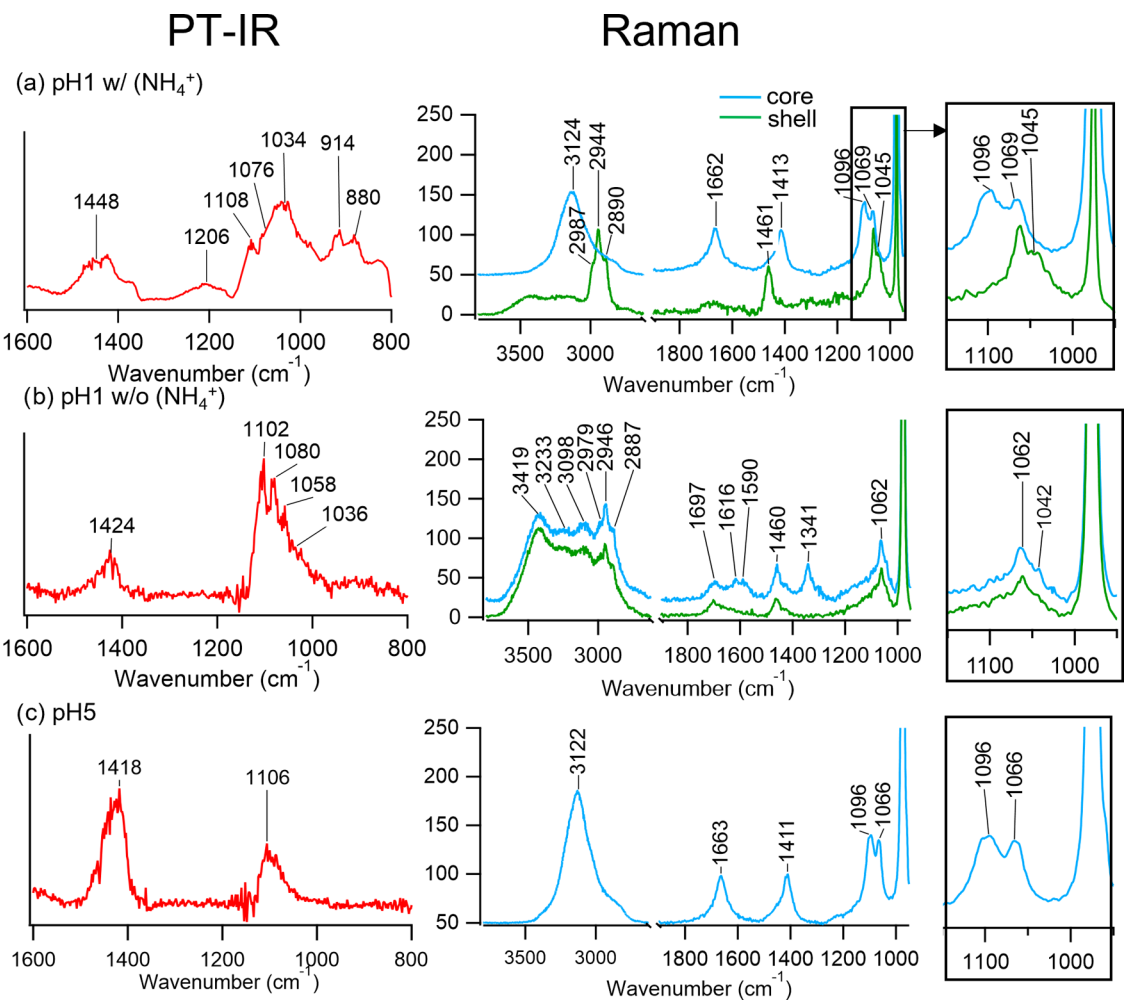

Figure 5. Representative PTIR spectra of individual particles after IEPOX reactive uptake for 60 min: (a) pH 1 (NH_4^+, HSO_4^- ≫ SO_4^-, H^+, H_2O), (b) pH 1 (HSO_4^- ≫ SO_4^-, H^+, H_2O) (red solid circle), and (c) pH 5 (NH_4^+, H^+, SO_4^{2-}, H_2O) (left column). Raman spectra of four different types of SOA particles after IEPOX uptake for 60 min showing composition differences between core and shell (right column).

1060 cm^{-1} in the Raman spectra indicative of $\nu_s(RO-SO_3^-)$ and 1200 cm^{-1} from $\nu_a(RO-SO_3^-)$ in the PTIR.[45] Other organic peaks were observed for both core and shell; specifically, the asymmetric carbon-hydrogen bend, $\delta(CH_2)$, of the methylene at 1460 cm^{-1},[45,93] symmetric and antisymmetric of methyl and methylene stretches were observed in the $\nu(C-H)$ region between 2800 to 3000 cm^{-1},[55,90] and carbonyl $\nu(C=O)$ at 1662 cm^{-1}. The hydroxyl $\nu(O-H)$ peak was observed at 3419 cm^{-1} from either the IEPOX uptake reaction or water from the aqueous core of the liquid particle.[90,94] The Raman spectra of particle core and shell show that more organic compounds were formed in the particle shell with a small amount of organics in the particle core, indicating that the gaseous IEPOX diffused through the shell of the particle to react and modify its physiochemical properties. A previous study has shown that aerosol acidity and viscosity can change drastically after seed aerosol has reacted with IEPOX, which can also inhibit additional multiphase chemical reactions of IEPOX.[54] Additionally, a PTIR spectrum was collected to provide complementary chemical composition information of an individual submicron particle. A strong asymmetric sulfate $\nu_{as}(SO_4^{2-})$ peak at 1108 cm^{-1} was observed.[78] The peak at 1206 cm^{-1} is assigned to bisulfate $\nu(HSO_4^-)$ and the peak at 1422 cm^{-1} is assigned to ammonium band $\delta(NH_4^+)$.[78] The peaks at 880, 914, and 1034 cm^{-1} have been identified as from the organosulfate group $\nu_s(RO-SO_3^-)$.

3.5. Characterization of Individual SOA Particles with Varying Initial Seed Aerosol Acidities. To further understand how the pH of seed particles affects gaseous IEPOX uptake, single-particle chemical composition was characterized using PTIR and Raman microspectroscopy at the highest and lowest pH values. Due to particle-to-particle variance, an average of 20 PTIR spectra and 15 Raman spectra were collected for each sample, with representative spectra shown in Figure 5. Organosulfate formation was observed in both the PTIR and Raman spectra after different acidic seed particles were exposed to gaseous IEPOX for 60 min. Organosulfates were identified by vibrational modes at 914, 1034, and 1206 cm^{-1}.[45] Different organosulfate vibrational modes can be either different organosulfates or different amounts of their corresponding dimer, trimer, or other oligomer, which will be probed in a future study. The reacted pH 1 seed particles with and without NH_4^+ formed more organosulfates, followed by the pH 1 seed particles and then pH 5 seed particles (Figure 5a–c). At the higher seed pH of 5, the formation of organosulfates decreased and more sulfate remained (Figure 5c). A more distinct difference between the core and shell spectra was observed when ammonium was present in the initial seed aerosol. We hypothesize that higher

https://doi.org/10.1021/acs.est.2c01579
Environ. Sci. Technol. 2022, 56, 10596−10607

ionic strength due to the presence of the ammonium ion may have enhanced the salting out and caused the eventual phase separation leading to the more distinct core and shell spectra in Figure 5a than for the particles without ammonium in the initial core in Figure 5b. This result is consistent with previous studies that showed SOA formation is significantly higher under acidic conditions.[49,66] Peaks in the PTIR spectra at ~1100 and 1418 cm^{-1} are assigned to antisymmetric sulfate stretches, $\nu_{as}(SO_4^{2-})$, and ammonium bending modes δ-(NH_4^+), respectively, with primarily $\nu_{as}(SO_4^{2-})$ observed when few organosulfates are present at pH 5.[78]

Raman spectra were collected in the particle core and shell to explore chemical differences. All SOA particles formed from seed particles with different pHs showed modes indicative of organosulfate formation, with peaks around 1065 cm^{-1}.[45] The distinctly different Raman spectra for particle cores and shells demonstrate chemically that phase separation occurred under acidic conditions (Figure 5a,b). The bisulfate $\nu(HSO_4^-)$ mode was observed at 1041 cm^{-1} for all acidic seed particles with pH 1 after IEPOX uptake, which suggests that the remaining aqueous component within particles remained acidic after exposure to IEPOX.[80,94,95] Though much smaller than the symmetric stretch in Raman, the antisymmetric sulfate $\nu_{as}(SO_4^{2-})$ mode at 1096 cm^{-1} was observed for the seed particles containing ammonium sulfate.[96] Lastly, for pH 1 and pH 3 seed particles with NH_4^+, the ν(N−H) peak around 3124 cm^{-1} was observed only in the particle core[97,98] and peaks in the ν(C−H) region between 2800 and 3000 cm^{-1} indicate that organic materials were present in the particle shell. Both PTIR and Raman spectra provide complementary information regarding the morphology and chemical composition after IEPOX multiphase chemical reactions.

3.6. Organosulfate Formation and Morphology Evolution during IEPOX Uptake. As organosulfate formation is consistently observed in IEPOX-derived SOA particles,[47] it is important to quantify the amount of organosulfates produced for each different seed pH. Figure 6 shows that organosulfate formation was observed under all pH conditions, with a strong pH dependence leading to rapid conversion of inorganic sulfate to organosulfates under the most acidic conditions (pH 1). Organosulfate formation is higher with NH_4^+ at pH 1, as the NH_4^+ may help stabilize the particle pH, preventing pH from decreasing after generation. Since pH may decrease less, less sulfate is protonated to bisulfate (below the pK_a), which is a weaker nucleophile,[99] which may slow organosulfate formation. The Raman spectra in Figure 5 also show more sulfate ($\nu_a(SO_4^{2-})$ = 1096 cm^{-1}) in pH 1 seed particles with NH_4^+ than pH 1 seed particles without NH_4^+, supporting this hypothesis. For less acidic aerosol conditions (pH 3 and 5), organosulfate production was much slower due to lower $[H^+]$, which is needed to facilitate the epoxide ring-opening reactions. This and prior experimental studies are buttressed by computational chemistry modeling that predicts that IEPOX rapidly produces organosulfates in acidic aerosols.[100] The results from this study show that most inorganic sulfate was converted to organosulfates within 60 min under acidic conditions (Figure 6a), and may indicate a self-limiting effect toward further IEPOX uptake at reaction times longer than 60 min.[54] For the less acidic inorganic seed particles, the maximum formation of organosulfates was observed within 80−100 min before stabilization. To further understand the particle morphology and phase impacts on organosulfate formation, AFM phase images were collected after 30-, 60-, and 120-min of reaction. Core−shell morphology was observed for each experiment across the different reaction times (Figures 6b−e), with thicker shells at lower pH where greater organosulfates are seen to form in Figure 6a. After the formation of a thicker shell (likely more viscous) and more solid core, the amount of organosulfate formation decreased.[33,55] It should be noted that by 120 min, the SOA coating on the particles formed with the pH 1 seed particles (with NH_4^+) was so thick that the core−shell morphology became difficult to resolve via phase imaging.

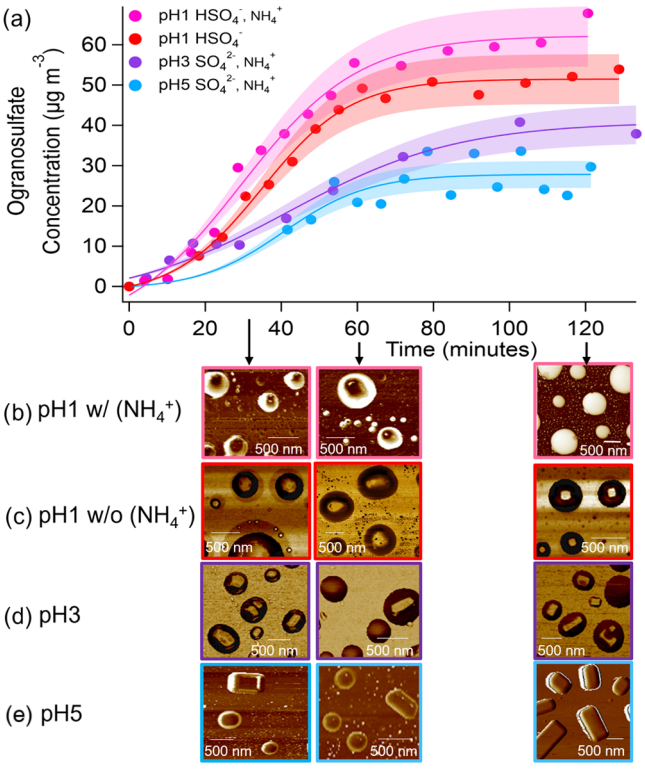

Figure 6. (a) Organosulfate concentrations by conversion of inorganic sulfate during the reactive uptake of IEPOX via ion chromatography measurement; the different color lines and shades represent sigmoid fit with uncertainties under different acidic conditions, and the data have been corrected for particle wall loss; and (b−e) AFM phase images of seed particles with varying pH reacted with gaseous IEPOX for 30, 60, and 120 min. Different colors correspond to different seed particles. Images for pH 3 and pH 5 are from repeat experiments due to a lack of sample availability from initial experiments shown in part (a).

This study demonstrates that the initial acidity and composition of inorganic seed particles impact their ultimate physicochemical properties (i.e., morphology and phase state) after exposure to gaseous IEPOX, which influences the continued formation, evolution, and reactivity of IEPOX-derived SOA. Phase separation was more pronounced under more acidic conditions, showing a clear core−shell morphology for individual submicron SOA particles. We further demonstrate that after reactive uptake of IEPOX on seed particles, the phase state of SOA particles shifts from a liquid phase to a semisolid or solid phase, even at 50% RH. This builds on prior work showing that aerosol physicochemical properties change dramatically with IEPOX uptake at different pH.[32,34,55,101] To further understand how acidity impacts the mechanism of organosulfate formation, future studies are needed that probe additional variables (e.g., RH and size). This

https://doi.org/10.1021/acs.est.2c01579
Environ. Sci. Technol. 2022, 56, 10596−10607

study clearly demonstrates a significant modification of morphology and phase evolution during IEPOX uptake onto seed particles with varying aerosol acidities. As aerosols from a range of sources with different initial pH values can form SOA leading to complex aerosol mixing states,[69,102−105] the strong effect of acidity on IEPOX-derived SOA physical and chemical properties may have substantial implications on SOA in isoprene-rich regions.[104,106−108] In the atmosphere, additional VOC oxidation products will be present, many from higher molecular weight VOCs (e.g., α-pinene). These SOA can be more viscous;[32,109,110] however, in a recent study, mixing of less viscous IEPOX-derived SOA with more viscous α-pinene and β-caryophyllene SOA decreased the overall SOA particle viscosity.[101] These results provide further evidence of the importance of considering acidity and phase for IEPOX-derived SOA. Initial efforts to model related effects have begun,[56] but further work is needed to fully account for this in regional- and global-scale models.

■ ASSOCIATED CONTENT

Supporting Information

The Supporting Information is available free of charge at https://pubs.acs.org/doi/10.1021/acs.est.2c01579.

Size distribution for four types of seed particles with varying pH and after IEPOX uptake (Figure S1); initial sulfate concentration of a seed aerosol only experiment (Figure S2); relative fraction of the HSO_4^- and SO_4^{2-} ions as a function of pH (Figure S3); concentration of 2-methyltetrols (2-MT) and their OS derivatives (2-methyltetrol sulfates, 2-MTSs) for SOA particles formed from pH 1 seed particles without ammonium (Figure S4); SEM images for four types of seed particles with varying pH reacted with IEPOX for 60 min (Figure S5); experimentally determined Raman and PTIR modes and tentative assignments for pH 1 ammonium bisulfate particle after IEPOX uptake for 60 min (Table S1) (PDF)

■ AUTHOR INFORMATION

Corresponding Authors

Jason D. Surratt − *Department of Environmental Sciences and Engineering, Gillings School of Global Public Health, The University of North Carolina at Chapel Hill, Chapel Hill, North Carolina 27599, United States; Department of Chemistry, University of North Carolina at Chapel Hill, Chapel Hill, North Carolina 27599, United States;* orcid.org/0000-0002-6833-1450; Email: surratt@unc.edu

Andrew P. Ault − *Department of Chemistry, University of Michigan, Ann Arbor, Michigan 48109, United States;* orcid.org/0000-0002-7313-8559; Email: aulta@umich.edu

Authors

Ziying Lei − *Department of Environmental Health Sciences, University of Michigan, Ann Arbor, Michigan 48109, United States;* Present Address: Department of Atmospheric Science, Texas A&M University, College Station, Texas, 77843, United States; orcid.org/0000-0003-3071-0698

Yuzhi Chen − *Department of Environmental Sciences and Engineering, Gillings School of Global Public Health, The University of North Carolina at Chapel Hill, Chapel Hill, North Carolina 27599, United States*

Yue Zhang − *Department of Environmental Sciences and Engineering, Gillings School of Global Public Health, The University of North Carolina at Chapel Hill, Chapel Hill, North Carolina 27599, United States;* Present Address: Department of Atmospheric Science, Texas A&M University, College Station, Texas, 77843, United States; orcid.org/0000-0001-7234-9672

Madeline E. Cooke − *Department of Chemistry, University of Michigan, Ann Arbor, Michigan 48109, United States*

Isabel R. Ledsky − *Department of Chemistry, Carleton College, Northfield, Minnesota 55057, United States*

N. Cazimir Armstrong − *Department of Environmental Sciences and Engineering, Gillings School of Global Public Health, The University of North Carolina at Chapel Hill, Chapel Hill, North Carolina 27599, United States*

Nicole E. Olson − *Department of Chemistry, University of Michigan, Ann Arbor, Michigan 48109, United States;* orcid.org/0000-0003-1600-8050

Zhenfa Zhang − *Department of Environmental Sciences and Engineering, Gillings School of Global Public Health, The University of North Carolina at Chapel Hill, Chapel Hill, North Carolina 27599, United States*

Avram Gold − *Department of Environmental Sciences and Engineering, Gillings School of Global Public Health, The University of North Carolina at Chapel Hill, Chapel Hill, North Carolina 27599, United States*

Complete contact information is available at: https://pubs.acs.org/10.1021/acs.est.2c01579

Funding

This work was supported by the National Science Foundation under Grants CHE-1654149, AGS-1703019, and AGS-2040610 (A.P.A.), as well as AGS-1703535 and AGS-2039788 (J.D.S.). Y.Z. acknowledges support from an NSF Postdoctoral Fellowship (AGS-1524731) and the National Institute of Health (NIH) training grant T32ES007018. A.G., Z.Z., and J.D.S. also acknowledge support from NSF Grant No. AGS-2001027 (Gold, Zhang). M.E.C. was supported by an NSF Graduate Research Fellowship (NSF-GRFP) DGE-1841052.

Notes

The authors declare no competing financial interest.

■ ACKNOWLEDGMENTS

Prof. Barbara J. Turpin and her research group are gratefully acknowledged for the use of the PILS and IC capabilities during these studies. Electron microscopy was conducted at the Michigan Center for Materials Characterization (MC^2). The authors acknowledge initial testing on samples with Prof. Mark Banaszak Holl and Dr. Jing Zhang at the Monash University.

■ REFERENCES

(1) Seinfeld, J. H.; Pandis, S. N. *Atmospheric Chemistry and Physics*; John Wiley & Sons, Inc.: NJ, 2016; pp 325−352.

(2) Riva, M.; Bell, D. M.; Hansen, A. M. K.; Drozd, G. T.; Zhang, Z. F.; Gold, A.; Imre, D.; Surratt, J. D.; Glasius, M.; Zelenyuk, A. Effect of Organic Coatings, Humidity and Aerosol Acidity on Multiphase Chemistry of Isoprene Epoxydiols. *Environ. Sci. Technol.* **2016**, *50*, 5580−5588.

(3) Riva, M.; Budisulistiorini, S. H.; Zhang, Z.; Gold, A.; Thornton, J. A.; Turpin, B. J.; Surratt, J. D. Multiphase reactivity of gaseous hydroperoxide oligomers produced from isoprene ozonolysis in the presence of acidified aerosols. *Atmos. Environ.* **2017**, *152*, 314−322.
(4) Jimenez, J. L.; Canagaratna, M. R.; Donahue, N. M.; Prevot, A. S. H.; Zhang, Q.; Kroll, J. H.; DeCarlo, P. F.; Allan, J. D.; Coe, H.; Ng, N. L.; Aiken, A. C.; Docherty, K. S.; Ulbrich, I. M.; Grieshop, A. P.; Robinson, A. L.; Duplissy, J.; Smith, J. D.; Wilson, K. R.; Lanz, V. A.; Hueglin, C.; Sun, Y. L.; Tian, J.; Laaksonen, A.; Raatikainen, T.; Rautiainen, J.; Vaattovaara, P.; Ehn, M.; Kulmala, M.; Tomlinson, J. M.; Collins, D. R.; Cubison, M. J.; Dunlea, E. J.; Huffman, J. A.; Onasch, T. B.; Alfarra, M. R.; Williams, P. I.; Bower, K.; Kondo, Y.; Schneider, J.; Drewnick, F.; Borrmann, S.; Weimer, S.; Demerjian, K.; Salcedo, D.; Cottrell, L.; Griffin, R.; Takami, A.; Miyoshi, T.; Hatakeyama, S.; Shimono, A.; Sun, J. Y.; Zhang, Y. M.; Dzepina, K.; Kimmel, J. R.; Sueper, D.; Jayne, J. T.; Herndon, S. C.; Trimborn, A. M.; Williams, L. R.; Wood, E. C.; Middlebrook, A. M.; Kolb, C. E.; Baltensperger, U.; Worsnop, D. R. Evolution of Organic Aerosols in the Atmosphere. *Science* **2009**, *326*, 1525−1529.
(5) Kroll, J. H.; Seinfeld, J. H. Chemistry of secondary organic aerosol: Formation and evolution of low-volatility organics in the atmosphere. *Atmos. Environ.* **2008**, *42*, 3593−3624.
(6) Ng, N. L.; Canagaratna, M. R.; Zhang, Q.; Jimenez, J. L.; Tian, J.; Ulbrich, I. M.; Kroll, J. H.; Docherty, K. S.; Chhabra, P. S.; Bahreini, R.; Murphy, S. M.; Seinfeld, J. H.; Hildebrandt, L.; Donahue, N. M.; DeCarlo, P. F.; Lanz, V. A.; Prévôt, A. S. H.; Dinar, E.; Rudich, Y.; Worsnop, D. R. Organic aerosol components observed in Northern Hemispheric datasets from Aerosol Mass Spectrometry. *Atmos. Chem. Phys.* **2010**, *10*, 4625−4641.
(7) Hallquist, M.; Wenger, J. C.; Baltensperger, U.; Rudich, Y.; Simpson, D.; Claeys, M.; Dommen, J.; Donahue, N. M.; George, C.; Goldstein, A. H.; Hamilton, J. F.; Herrmann, H.; Hoffmann, T.; Iinuma, Y.; Jang, M.; Jenkin, M. E.; Jimenez, J. L.; Kiendler-Scharr, A.; Maenhaut, W.; McFiggans, G.; Mentel, T. F.; Monod, A.; Prevot, A. S. H.; Seinfeld, J. H.; Surratt, J. D.; Szmigielski, R.; Wildt, J. The formation, properties and impact of secondary organic aerosol: current and emerging issues. *Atmos. Chem. Phys.* **2009**, *9*, 5155−5236.
(8) Zhang, H.; Yee, L. D.; Lee, B. H.; Curtis, M. P.; Worton, D. R.; Isaacman-VanWertz, G.; Offenberg, J. H.; Lewandowski, M.; Kleindienst, T. E.; Beaver, M. R.; et al. Monoterpenes are the largest source of summertime organic aerosol in the southeastern United States. *Proc. Natl. Acad. Sci. U.S.A.* **2018**, *115*, 2038−2043.
(9) Huang, R.-J.; Zhang, Y.; Bozzetti, C.; Ho, K.-F.; Cao, J.-J.; Han, Y.; Daellenbach, K. R.; Slowik, J. G.; Platt, S. M.; Canonaco, F.; et al. High secondary aerosol contribution to particulate pollution during haze events in China. *Nature* **2014**, *514*, 218−222.
(10) Tsimpidi, A. P.; Karydis, V. A.; Pandis, S. N.; Lelieveld, J. Global combustion sources of organic aerosols: model comparison with 84 AMS factor-analysis data sets. *Atmos. Chem. Phys.* **2016**, *16*, 8939−8962.
(11) Pye, H. O. T.; Ward-Caviness, C. K.; Murphy, B. N.; Appel, K. W.; Seltzer, K. M. Secondary organic aerosol association with cardiorespiratory disease mortality in the United States. *Nat. Commun.* **2021**, *12*, No. 7215.
(12) Arashiro, M.; Lin, Y.-H.; Zhang, Z.; Sexton, K. G.; Gold, A.; Jaspers, I.; Fry, R. C.; Surratt, J. D. Effect of secondary organic aerosol from isoprene-derived hydroxyhydroperoxides on the expression of oxidative stress response genes in human bronchial epithelial cells. *Environ. Sci.: Processes Impacts* **2018**, *20*, 332−339.
(13) Khan, F.; Kwapiszewska, K.; Zhang, Y.; Chen, Y.; Lambe, A. T.; Kołodziejczyk, A.; Jalal, N.; Rudzinski, K.; Martínez-Romero, A.; Fry, R. C.; Surratt, J. D.; Szmigielski, R. Toxicological responses of α-pinene-derived secondary organic aerosol and its molecular tracers in human lung cell lines. *Chem. Res. Toxicol.* **2021**, *34*, 817−832.
(14) Chowdhury, P. H.; He, Q.; Lasitza Male, T.; Brune, W. H.; Rudich, Y.; Pardo, M. Exposure of lung epithelial cells to photochemically aged secondary organic aerosol shows increased toxic effects. *Environ. Sci. Technol. Lett.* **2018**, *5*, 424−430.
(15) Chowdhury, P. H.; He, Q.; Carmieli, R.; Li, C.; Rudich, Y.; Pardo, M. Connecting the oxidative potential of secondary organic aerosols with reactive oxygen species in exposed lung cells. *Environ. Sci. Technol.* **2019**, *53*, 13949−13958.
(16) Surratt, J. D.; L, Y.-H.; Arashiro, M.; Vizuete, W. G.; Zhang, Z.; Gold, A.; Jaspers, I.; Fry, R. C. *Understanding the Early Biological Effects of Isoprene-Derived Particulate Matter Enhanced by Anthropogenic Pollutants*; Health Effects Institute: Boston, Massachusetts, 2019.
(17) Guenther, A.; Jiang, X.; Shah, T.; Huang, L.; Kemball-Cook, S.; Yarwood, G. *Model of Emissions of Gases and Aerosol from Nature Version 3 (MEGAN3) for Estimating Biogenic Emissions*; Mensink, C.; Gong, W.; Hakami, A., Eds.; Air Pollution Modeling and its Application XXVI, Cham, 2020//, 2020; Springer International Publishing: Cham, 2020; pp 187−192.
(18) Guenther, A.; Karl, T.; Harley, P.; Wiedinmyer, C.; Palmer, P. I.; Geron, C. Estimates of global terrestrial isoprene emissions using MEGAN (Model of Emissions of Gases and Aerosols from Nature). *Atmos. Chem. Phys.* **2006**, *6*, 3181−3210.
(19) Paulot, F.; Crounse, J. D.; Kjaergaard, H. G.; Kurten, A.; St Clair, J. M.; Seinfeld, J. H.; Wennberg, P. O. Unexpected Epoxide Formation in the Gas-Phase Photooxidation of Isoprene. *Science* **2009**, *325*, 730−733.
(20) Bates, K. H.; Crounse, J. D.; St Clair, J. M.; Bennett, N. B.; Nguyen, T. B.; Seinfeld, J. H.; Stoltz, B. M.; Wennberg, P. O. Gas Phase Production and Loss of Isoprene Epoxydiols. *J. Phys. Chem. A* **2014**, *118*, 1237−1246.
(21) Zhang, Y.; Nichman, L.; Spencer, P.; Jung, J. I.; Lee, A.; Heffernan, B. K.; Gold, A.; Zhang, Z.; Chen, Y.; Canagaratna, M. R.; Jayne, J. T.; Worsnop, D. R.; Onasch, T. B.; Surratt, J. D.; Chandler, D.; Davidovits, P.; Kolb, C. E. The Cooling Rate- and Volatility-Dependent Glass-Forming Properties of Organic Aerosols Measured by Broadband Dielectric Spectroscopy. *Environ. Sci. Technol.* **2019**, *53*, 12366−12378.
(22) Carlton, A. G.; Wiedinmyer, C.; Kroll, J. H. A review of Secondary Organic Aerosol (SOA) formation from isoprene. *Atmos. Chem. Phys.* **2009**, *9*, 4987−5005.
(23) Gaston, C. J.; Riedel, T. P.; Zhang, Z. F.; Gold, A.; Surratt, J. D.; Thornton, J. A. Reactive Uptake of an Isoprene-Derived Epoxydiol to Submicron Aerosol Particles. *Environ. Sci. Technol.* **2014**, *48*, 11178−11186.
(24) Riedel, T. P.; Lin, Y. H.; Budisulistiorini, H.; Gaston, C. J.; Thornton, J. A.; Zhang, Z. F.; Vizuete, W.; Gold, A.; Surrattt, J. D. Heterogeneous Reactions of Isoprene-Derived Epoxides: Reaction Probabilities and Molar Secondary Organic Aerosol Yield Estimates. *Environ. Sci. Technol. Lett.* **2015**, *2*, 38−42.
(25) Jang, M.; Czoschke, N. M.; Lee, S.; Kamens, R. M. Heterogeneous Atmospheric Aerosol Production by Acid-Catalyzed Particle-Phase Reactions. *Science* **2002**, *298*, 814−817.
(26) Czoschke, N. M.; Jang, M.; Kamens, R. M. Effect of acidic seed on biogenic secondary organic aerosol growth. *Atmos. Environ.* **2003**, *37*, 4287−4299.
(27) Budisulistiorini, S. H.; Baumann, K.; Edgerton, E. S.; Bairai, S. T.; Mueller, S.; Shaw, S. L.; Knipping, E. M.; Gold, A.; Surratt, J. D. Seasonal characterization of submicron aerosol chemical composition and organic aerosol sources in the southeastern United States: Atlanta, Georgia,and Look Rock, Tennessee. *Atmos. Chem. Phys.* **2016**, *16*, 5171−5189.
(28) Xu, L.; Guo, H.; Boyd, C. M.; Klein, M.; Bougiatioti, A.; Cerully, K. M.; Hite, J. R.; Isaacman-VanWertz, G.; Kreisberg, N. M.; Knote, C.; Olson, K.; Koss, A.; Goldstein, A. H.; Hering, S. V.; de Gouw, J.; Baumann, K.; Lee, S.-H.; Nenes, A.; Weber, R. J.; Ng, N. L. Effects of anthropogenic emissions on aerosol formation from isoprene and monoterpenes in the southeastern United States. *Proc. Natl. Acad. Sci. U.S.A.* **2015**, *112*, 37−42.
(29) Budisulistiorini, S. H.; Li, X.; Bairai, S. T.; Renfro, J.; Liu, Y.; Liu, Y. J.; McKinney, K. A.; Martin, S. T.; McNeill, V. F.; Pye, H. O. T.; Nenes, A.; Neff, M. E.; Stone, E. A.; Mueller, S.; Knote, C.; Shaw, S. L.; Zhang, Z.; Gold, A.; Surratt, J. D. Examining the effects of anthropogenic emissions on isoprene-derived secondary organic

https://doi.org/10.1021/acs.est.2c01579
Environ. Sci. Technol. 2022, 56, 10596−10607

aerosol formation during the 2013 Southern Oxidant and Aerosol Study (SOAS) at the Look Rock, Tennessee ground site. *Atmos. Chem. Phys.* **2015**, *15*, 8871−8888.
(30) Budisulistiorini, S. H.; Canagaratna, M. R.; Croteau, P. L.; Marth, W. J.; Baumann, K.; Edgerton, E. S.; Shaw, S. L.; Knipping, E. M.; Worsnop, D. R.; Jayne, J. T.; Gold, A.; Surratt, J. D. Real-Time Continuous Characterization of Secondary Organic Aerosol Derived from Isoprene Epoxydiols in Downtown Atlanta, Georgia, Using the Aerodyne Aerosol Chemical Speciation Monitor. *Environ. Sci. Technol.* **2013**, *47*, 5686−5694.
(31) Hu, W. W.; Campuzano-Jost, P.; Palm, B. B.; Day, D. A.; Ortega, A. M.; Hayes, P. L.; Krechmer, J. E.; Chen, Q.; Kuwata, M.; Liu, Y. J.; de Sa, S. S.; McKinney, K.; Martin, S. T.; Hu, M.; Budisulistiorini, S. H.; Riva, M.; Surratt, J. D.; St Clair, J. M.; Isaacman-Van Wertz, G.; Yee, L. D.; Goldstein, A. H.; Carbone, S.; Brito, J.; Artaxo, P.; de Gouw, J. A.; Koss, A.; Wisthaler, A.; Mikoviny, T.; Karl, T.; Kaser, L.; Jud, W.; Hansel, A.; Docherty, K. S.; Alexander, M. L.; Robinson, N. H.; Coe, H.; Allan, J. D.; Canagaratna, M. R.; Paulot, F.; Jimenez, J. L. Characterization of a real-time tracer for isoprene epoxydiols-derived secondary organic aerosol (IEPOX-SOA) from aerosol mass spectrometer measurements. *Atmos. Chem. Phys.* **2015**, *15*, 11807−11833.
(32) Slade, J. H.; Ault, A. P.; Bui, A. T.; Ditto, J. C.; Lei, Z.; Bondy, A. L.; Olson, N. E.; Cook, R. D.; Desrochers, S. J.; Harvey, R. M.; Erickson, M. H.; Wallace, H. W.; Alvarez, S. L.; Flynn, J. H.; Boor, B. E.; Petrucci, G. A.; Gentner, D. R.; Griffin, R. J.; Shepson, P. B. Bouncier Particles at Night: Biogenic Secondary Organic Aerosol Chemistry and Sulfate Drive Diel Variations in the Aerosol Phase in a Mixed Forest. *Environ. Sci. Technol.* **2019**, *53*, 4977−4987.
(33) Zhang, Y.; Chen, Y.; Lambe, A. T.; Olson, N. E.; Lei, Z.; Craig, R. L.; Zhang, Z.; Gold, A.; Onasch, T. B.; Jayne, J. T.; Worsnop, D. R.; Gaston, C. J.; Thornton, J. A.; Vizuete, W.; Ault, A. P.; Surratt, J. D. Effect of the Aerosol-Phase State on Secondary Organic Aerosol Formation from the Reactive Uptake of Isoprene-Derived Epoxydiols (IEPOX). *Environ. Sci. Technol. Lett.* **2018**, *5*, 167−174.
(34) Riva, M.; Chen, Y.; Zhang, Y.; Lei, Z.; Olson, N. E.; Boyer, H. C.; Narayan, S.; Yee, L. D.; Green, H. S.; Cui, T.; Zhang, Z.; Baumann, K.; Fort, M.; Edgerton, E.; Budisulistiorini, S. H.; Rose, C. A.; Ribeiro, I. O.; e Oliveira, R. L.; dos Santos, E. O.; Machado, C. M. D.; Szopa, S.; Zhao, Y.; Alves, E. G.; de Sá, S. S.; Hu, W.; Knipping, E. M.; Shaw, S. L.; Duvoisin Junior, S.; de Souza, R. A. F.; Palm, B. B.; Jimenez, J.-L.; Glasius, M.; Goldstein, A. H.; Pye, H. O. T.; Gold, A.; Turpin, B. J.; Vizuete, W.; Martin, S. T.; Thornton, J. A.; Dutcher, C. S.; Ault, A. P.; Surratt, J. D. Increasing Isoprene Epoxydiol-to-Inorganic Sulfate Aerosol Ratio Results in Extensive Conversion of Inorganic Sulfate to Organosulfur Forms: Implications for Aerosol Physicochemical Properties. *Environ. Sci. Technol.* **2019**, *53*, 8682−8694.
(35) Chan, L. P.; Chan, C. K. Role of the aerosol phase state in ammonia/amines exchange reactions. *Environ. Sci. Technol.* **2013**, *47*, 5755−5762.
(36) Pajunoja, A.; Hu, W.; Leong, Y. J.; Taylor, N. F.; Miettinen, P.; Palm, B. B.; Mikkonen, S.; Collins, D. R.; Jimenez, J. L.; Virtanen, A. Phase state of ambient aerosol linked with water uptake and chemical aging in the southeastern US. *Atmos. Chem. Phys.* **2016**, *16*, 11163−11176.
(37) Kirpes, R. M.; Lei, Z.; Fraund, M.; Gunsch, M. J.; May, N. W.; Barrett, T. E.; Moffett, C. E.; Schauer, A. J.; Alexander, B.; Upchurch, L. M.; China, S.; Quinn, P. K.; Moffet, R. C.; Laskin, A.; Sheesley, R. J.; Pratt, K. A.; Ault, A. P. Solid organic-coated ammonium sulfate particles at high relative humidity in the summertime Arctic atmosphere. *Proc. Natl. Acad. Sci. U.S.A.* **2022**, *119*, No. e2104496119.
(38) Koop, T.; Bookhold, J.; Shiraiwa, M.; Poschl, U. Glass transition and phase state of organic compounds: dependency on molecular properties and implications for secondary organic aerosols in the atmosphere. *Phys. Chem. Chem. Phys.* **2011**, *13*, 19238−19255.
(39) Martin, S. T. Phase transitions of aqueous atmospheric particles. *Chem. Rev.* **2000**, *100*, 3403−3454.
(40) Maclean, A. M.; Smith, N. R.; Li, Y.; Huang, Y.; Hettiyadura, A. P.; Crescenzo, G. V.; Shiraiwa, M.; Laskin, A.; Nizkorodov, S. A.; Bertram, A. K. Humidity-Dependent Viscosity of Secondary Organic Aerosol from Ozonolysis of β-Caryophyllene: Measurements, Predictions, and Implications. *ACS Earth Space Chem.* **2021**, *5*, 305−318.
(41) Pajunoja, A.; Malila, J.; Hao, L.; Joutsensaari, J.; Lehtinen, K. E.; Virtanen, A. Estimating the viscosity range of SOA particles based on their coalescence time. *Aerosol Sci. Technol.* **2014**, *48*, i−iv.
(42) Renbaum-Wolff, L.; Grayson, J. W.; Bateman, A. P.; Kuwata, M.; Sellier, M.; Murray, B. J.; Shilling, J. E.; Martin, S. T.; Bertram, A. K. Viscosity of alpha-pinene secondary organic material and implications for particle growth and reactivity. *Proc. Natl. Acad. Sci. U.S.A.* **2013**, *110*, 8014−8019.
(43) Song, M.; Liu, P. F.; Hanna, S. J.; Zaveri, R. A.; Potter, K.; You, Y.; Martin, S. T.; Bertram, A. K. Relative humidity-dependent viscosity of secondary organic material from toluene photo-oxidation and possible implications for organic particulate matter over megacities. *Atmos. Chem. Phys.* **2016**, *16*, 8817−8830.
(44) Surratt, J. D.; Chan, A. W. H.; Eddingsaas, N. C.; Chan, M. N.; Loza, C. L.; Kwan, A. J.; Hersey, S. P.; Flagan, R. C.; Wennberg, P. O.; Seinfeld, J. H. Reactive intermediates revealed in secondary organic aerosol formation from isoprene. *Proc. Natl. Acad. Sci. U.S.A.* **2010**, *107*, 6640−6645.
(45) Bondy, A. L.; Craig, R. L.; Zhang, Z.; Gold, A.; Surratt, J. D.; Ault, A. P. Isoprene-Derived Organosulfates: Vibrational Mode Analysis by Raman Spectroscopy, Acidity-Dependent Spectral Modes, and Observation in Individual Atmospheric Particles. *J. Phys. Chem. A* **2018**, *122*, 303−315.
(46) Budisulistiorini, S. H.; Nenes, A.; Carlton, A. G.; Surratt, J. D.; McNeill, V. F.; Pye, H. O. Simulating aqueous-phase isoprene-epoxydiol (IEPOX) secondary organic aerosol production during the 2013 Southern Oxidant and Aerosol Study (SOAS). *Environ. Sci. Technol.* **2017**, *51*, 5026−5034.
(47) Surratt, J. D.; Gomez-Gonzalez, Y.; Chan, A. W. H.; Vermeylen, R.; Shahgholi, M.; Kleindienst, T. E.; Edney, E. O.; Offenberg, J. H.; Lewandowski, M.; Jaoui, M.; Maenhaut, W.; Claeys, M.; Flagan, R. C.; Seinfeld, J. H. Organosulfate formation in biogenic secondary organic aerosol. *J. Phys. Chem. A* **2008**, *112*, 8345−8378.
(48) Surratt, J. D.; Murphy, S. M.; Kroll, J. H.; Ng, N. L.; Hildebrandt, L.; Sorooshian, A.; Szmigielski, R.; Vermeylen, R.; Maenhaut, W.; Claeys, M.; Flagan, R. C.; Seinfeld, J. H. Chemical composition of secondary organic aerosol formed from the photo-oxidation of isoprene. *J. Phys. Chem. A* **2006**, *110*, 9665−9690.
(49) Lin, Y. H.; Zhang, Z. F.; Docherty, K. S.; Zhang, H. F.; Budisulistiorini, S. H.; Rubitschun, C. L.; Shaw, S. L.; Knipping, E. M.; Edgerton, E. S.; Kleindienst, T. E.; Gold, A.; Surratt, J. D. Isoprene Epoxydiols as Precursors to Secondary Organic Aerosol Formation: Acid-Catalyzed Reactive Uptake Studies with Authentic Compounds. *Environ. Sci. Technol.* **2012**, *46*, 250−258.
(50) Claeys, M.; Graham, B.; Vas, G.; Wang, W.; Vermeylen, R.; Pashynska, V.; Cafmeyer, J.; Guyon, P.; Andreae, M. O.; Artaxo, P.; Maenhaut, W. Formation of secondary organic aerosols through photooxidation of isoprene. *Science* **2004**, *303*, 1173−1176.
(51) Claeys, M.; Wang, W.; Ion, A. C.; Kourtchev, I.; Gelencsér, A.; Maenhaut, W. Formation of secondary organic aerosols from isoprene and its gas-phase oxidation products through reaction with hydrogen peroxide. *Atmos. Environ.* **2004**, *38*, 4093−4098.
(52) Lin, Y. H.; Budisulistiorini, H.; Chu, K.; Siejack, R. A.; Zhang, H. F.; Riva, M.; Zhang, Z. F.; Gold, A.; Kautzman, K. E.; Surratt, J. D. Light-Absorbing Oligomer Formation in Secondary Organic Aerosol from Reactive Uptake of Isoprene Epoxydiols. *Environ. Sci. Technol.* **2014**, *48*, 12012−12021.
(53) Tolocka, M. P.; Jang, M.; Ginter, J. M.; Cox, F. J.; Kamens, R. M.; Johnston, M. V. Formation of oligomers in secondary organic aerosol. *Environ. Sci. Technol.* **2004**, *38*, 1428−1434.
(54) Zhang, Y.; Chen, Y.; Lei, Z.; Olson, N.; Riva, M.; Koss, A. R.; Zhang, Z.; Gold, A.; Jayne, J. T.; Worsnop, D. R.; Onasch, T. B.; Kroll, J. H.; Turpin, B. J.; Ault, A. P.; Surratt, J. D. Joint Impacts of

https://doi.org/10.1021/acs.est.2c01579
Environ. Sci. Technol. 2022, 56, 10596−10607

Acidity and Viscosity on the Formation of Secondary Organic Aerosol from Isoprene Epoxydiols (IEPOX) in Phase Separated Particles. *ACS Earth Space Chem.* **2019**, *3*, 2646−2658.
(55) Olson, N. E.; Lei, Z.; Craig, R. L.; Zhang, Y.; Chen, Y.; Lambe, A. T.; Zhang, Z.; Gold, A.; Surratt, J. D.; Ault, A. P. Reactive Uptake of Isoprene Epoxydiols Increases the Viscosity of the Core of Phase-Separated Aerosol Particles. *ACS Earth Space Chem.* **2019**, *3*, 1402−1414.
(56) Schmedding, R.; Rasool, Q. Z.; Zhang, Y.; Pye, H. O. T.; Zhang, H.; Chen, Y.; Surratt, J. D.; Lee, B. H.; Mohr, C.; Lopez-Hilfiker, F. D.; Thornton, J. A.; Goldstein, A. H.; Vizuete, W. Predicting Secondary Organic Aerosol Phase State and Viscosity and its Effect on Multiphase Chemistry in a Regional Scale Air Quality Model. *Atmos. Chem. Phys.* **2020**, *20*, 8201−8225.
(57) Veghte, D. P.; Altaf, M. B.; Freedman, M. A. Size Dependence of the Structure of Organic Aerosol. *J. Am. Chem. Soc.* **2013**, *135*, 16046−16049.
(58) Qiu, Y. Q.; Molinero, V. Morphology of Liquid-Liquid Phase Separated Aerosols. *J. Am. Chem. Soc.* **2015**, *137*, 10642−10651.
(59) O'Brien, R. E.; Wang, B.; Kelly, S. T.; Lundt, N.; You, Y.; Bertram, A. K.; Leone, S. R.; Laskin, A.; Gilles, M. K. Liquid−liquid phase separation in aerosol particles: Imaging at the nanometer scale. *Environ. Sci. Technol.* **2015**, *49*, 4995−5002.
(60) Lienhard, D. M.; Huisman, A. J.; Krieger, U. K.; Rudich, Y.; Marcolli, C.; Luo, B. P.; Bones, D. L.; Reid, J. P.; Lambe, A. T.; Canagaratna, M. R.; Davidovits, P.; Onasch, T. B.; Worsnop, D. R.; Steimer, S. S.; Koop, T.; Peter, T. Viscous organic aerosol particles in the upper troposphere: diffusivity-controlled water uptake and ice nucleation? *Atmos. Chem. Phys.* **2015**, *15*, 13599−13613.
(61) Zhou, S.; Hwang, B. C.; Lakey, P. S.; Zuend, A.; Abbatt, J. P.; Shiraiwa, M. Multiphase reactivity of polycyclic aromatic hydrocarbons is driven by phase separation and diffusion limitations. *Proc. Natl. Acad. Sci. U.S.A.* **2019**, *116*, 11658−11663.
(62) Drozd, G. T.; Woo, J. L.; McNeill, V. F. Self-limited uptake of alpha-pinene oxide to acidic aerosol: the effects of liquid-liquid phase separation and implications for the formation of secondary organic aerosol and organosulfates from epoxides. *Atmos. Chem. Phys.* **2013**, *13*, 8255−8263.
(63) Guo, H.; Otjes, R.; Schlag, P.; Kiendler-Scharr, A.; Nenes, A.; Weber, R. J. Effectiveness of ammonia reduction on control of fine particle nitrate. *Atmos. Chem. Phys.* **2018**, *18*, 12241−12256.
(64) Rindelaub, J. D.; McAvey, K. M.; Shepson, P. B. The photochemical production of organic nitrates from α-pinene and loss via acid-dependent particle phase hydrolysis. *Atmos. Environ.* **2015**, *100*, 193−201.
(65) Surratt, J. D.; Lewandowski, M.; Offenberg, J. H.; Jaoui, M.; Kleindienst, T. E.; Edney, E. O.; Seinfeld, J. H. Effect of acidity on secondary organic aerosol formation from isoprene. *Environ. Sci. Technol.* **2007**, *41*, 5363−5369.
(66) Jang, M. S.; Czoschke, N. M.; Lee, S.; Kamens, R. M. Heterogeneous atmospheric aerosol production by acid-catalyzed particle-phase reactions. *Science* **2002**, *298*, 814−817.
(67) Tang, Y. S.; Braban, C. F.; Dragosits, U.; Dore, A. J.; Simmons, I.; van Dijk, N.; Poskitt, J.; Dos Santos Pereira, G.; Keenan, P. O.; Conolly, C.; Vincent, K.; Smith, R. I.; Heal, M. R.; Sutton, M. A. Drivers for spatial, temporal and long-term trends in atmospheric ammonia and ammonium in the UK. *Atmos. Chem. Phys.* **2018**, *18*, 705−733.
(68) Meng, Z.; Xu, X.; Lin, W.; Ge, B.; Xie, Y.; Song, B.; Jia, S.; Zhang, R.; Peng, W.; Wang, Y.; Cheng, H.; Yang, W.; Zhao, H. Role of ambient ammonia in particulate ammonium formation at a rural site in the North China Plain. *Atmos. Chem. Phys.* **2018**, *18*, 167−184.
(69) Pye, H. O. T.; Nenes, A.; Alexander, B.; Ault, A. P.; Barth, M. C.; Clegg, S. L.; Collett, J. L., Jr; Fahey, K. M.; Hennigan, C. J.; Herrmann, H.; Kanakidou, M.; Kelly, J. T.; Ku, I. T.; McNeill, V. F.; Riemer, N.; Schaefer, T.; Shi, G.; Tilgner, A.; Walker, J. T.; Wang, T.; Weber, R.; Xing, J.; Zaveri, R. A.; Zuend, A. The acidity of atmospheric particles and clouds. *Atmos. Chem. Phys.* **2020**, *20*, 4809−4888.
(70) Pye, H. O. T.; Pinder, R. W.; Piletic, I. R.; Xie, Y.; Capps, S. L.; Lin, Y. H.; Surratt, J. D.; Zhang, Z. F.; Gold, A.; Luecken, D. J.; Hutzell, W. T.; Jaoui, M.; Offenberg, J. H.; Kleindienst, T. E.; Lewandowski, M.; Edney, E. O. Epoxide Pathways Improve Model Predictions of Isoprene Markers and Reveal Key Role of Acidity in Aerosol Formation. *Environ. Sci. Technol.* **2013**, *47*, 11056−11064.
(71) Dubois, C.; Cholleton, D.; Gemayel, R.; Chen, Y.; Surratt, J.; George, C.; Rairoux, P.; Miffre, A.; Riva, M. Decrease in sulfate aerosol light backscattering by reactive uptake of isoprene epoxydiols. *Phys. Chem. Chem. Phys.* **2021**, *23*, 5927−5935.
(72) Lambe, A. T.; Onasch, T. B.; Massoli, P.; Croasdale, D. R.; Wright, J. P.; Ahern, A. T.; Williams, L. R.; Worsnop, D. R.; Brune, W. H.; Davidovits, P. Laboratory studies of the chemical composition and cloud condensation nuclei (CCN) activity of secondary organic aerosol (SOA) and oxidized primary organic aerosol (OPOA). *Atmos. Chem. Phys.* **2011**, *11*, 8913−8928.
(73) Wolf, M. J.; Zhang, Y.; Zawadowicz, M. A.; Goodell, M.; Froyd, K.; Freney, E.; Sellegri, K.; Rösch, M.; Cui, T.; Winter, M.; Lacher, L.; Axisa, D.; DeMott, P. J.; Levin, E. J. T.; Gute, E.; Abbatt, J.; Koss, A.; Kroll, J. H.; Surratt, J. D.; Cziczo, D. J. A biogenic secondary organic aerosol source of cirrus ice nucleating particles. *Nat. Commun.* **2020**, *11*, No. 4834.
(74) Guo, H.; Xu, L.; Bougiatioti, A.; Cerully, K. M.; Capps, S. L.; Hite, J. R., Jr; Carlton, A. G.; Lee, S. H.; Bergin, M. H.; Ng, N. L.; Nenes, A.; Weber, R. J. Fine-particle water and pH in the southeastern United States. *Atmos. Chem. Phys.* **2015**, *15*, 5211−5228.
(75) Nenes, A.; Krom, M. D.; Mihalopoulos, N.; Van Cappellen, P.; Shi, Z.; Bougiatioti, A.; Zarmpas, P.; Herut, B. Atmospheric acidification of mineral aerosols: a source of bioavailable phosphorus for the oceans. *Atmos. Chem. Phys.* **2011**, *11*, 6265−6272.
(76) Battaglia, M. A., Jr; Douglas, S.; Hennigan, C. J. Effect of the urban heat island on aerosol pH. *Environ. Sci. Technol.* **2017**, *51*, 13095−13103.
(77) Zhang, Z.; Lin, Y. H.; Zhang, H.; Surratt, J. D.; Ball, L. M.; Gold, A. Technical Note: Synthesis of isoprene atmospheric oxidation products: isomeric epoxydiols and the rearrangement products *cis*- and *trans*-3-methyl-3,4-dihydroxytetrahydrofuran. *Atmos. Chem. Phys.* **2012**, *12*, 8529−8535.
(78) Bondy, A. L.; Kirpes, R. M.; Merzel, R. L.; Pratt, K. A.; Banaszak Holl, M. M.; Ault, A. P. Atomic Force Microscopy-Infrared Spectroscopy of Individual Atmospheric Aerosol Particles: Subdiffraction Limit Vibrational Spectroscopy and Morphological Analysis. *Anal. Chem.* **2017**, *89*, 8594−8598.
(79) Bondy, A. L.; Wang, B.; Laskin, A.; Craig, R. L.; Nhliziyo, M. V.; Bertman, S. B.; Pratt, K. A.; Shepson, P. B.; Ault, A. P. Inland Sea Spray Aerosol Transport and Incomplete Chloride Depletion: Varying Degrees of Reactive Processing Observed during SOAS. *Environ. Sci. Technol.* **2017**, *51*, 9533−9542.
(80) Craig, R. L.; Bondy, A. L.; Ault, A. P. Computer-controlled Raman microspectroscopy (CC-Raman): A method for the rapid characterization of individual atmospheric aerosol particles. *Aerosol Sci. Technol.* **2017**, *51*, 1099−1112.
(81) Riva, M.; Budisulistiorini, S. H.; Chen, Y.; Zhang, Z.; D'Ambro, E. L.; Zhang, X.; Gold, A.; Turpin, B. J.; Thornton, J. A.; Canagaratna, M. R.; Surratt, J. D. Chemical Characterization of Secondary Organic Aerosol from Oxidation of Isoprene Hydroxyhydroperoxides. *Environ. Sci. Technol.* **2016**, *50*, 9889−9899.
(82) Zhang, Y.; Chen, Y.; Lei, Z.; Olson, N. E.; Riva, M.; Koss, A. R.; Zhang, Z.; Gold, A.; Jayne, J. T.; Worsnop, D. R.; Onasch, T. B.; Kroll, J. H.; Turpin, B. J.; Ault, A. P.; Surratt, J. D. Joint Impacts of Acidity and Viscosity on the Formation of Secondary Organic Aerosol from Isoprene Epoxydiols (IEPOX) in Phase Separated Particles. *ACS Earth Space Chem.* **2019**, *3*, 2646−2658.
(83) Cui, T.; Zeng, Z.; dos Santos, E. O.; Zhang, Z.; Chen, Y.; Zhang, Y.; Rose, C. A.; Budisulistiorini, S. H.; Collins, L. B.; Bodnar, W. M.; de Souza, R. A. F.; Martin, S. T.; Machado, C. M. D.; Turpin, B. J.; Gold, A.; Ault, A. P.; Surratt, J. D. Development of a hydrophilic interaction liquid chromatography (HILIC) method for the chemical characterization of water-soluble isoprene epoxydiol (IEPOX)-derived

https://doi.org/10.1021/acs.est.2c01579
Environ. Sci. Technol. 2022, 56, 10596−10607

secondary organic aerosol. *Environ. Sci.: Processes Impacts* **2018**, *20*, 1524−1536.
(84) Imre, D. G.; Xu, J.; Tang, I.; McGraw, R. Ammonium bisulfate/water equilibrium and metastability phase diagrams. *J. Phys. Chem. A* **1997**, *101*, 4191−4195.
(85) Cziczo, D. J.; Abbatt, J. Deliquescence, efflorescence, and supercooling of ammonium sulfate aerosols at low temperature: Implications for cirrus cloud formation and aerosol phase in the atmosphere. *J. Geophys. Res.: Atmos.* **1999**, *104*, 13781−13790.
(86) Onasch, T. B.; Siefert, R. L.; Brooks, S. D.; Prenni, A. J.; Murray, B.; Wilson, M. A.; Tolbert, M. A. Infrared spectroscopic study of the deliquescence and efflorescence of ammonium sulfate aerosol as a function of temperature. *J. Geophys. Res.: Atmos.* **1999**, *104*, 21317−21326.
(87) Cheng, Z.; Sharma, N.; Tseng, K.-P.; Kovarik, L.; China, S. Direct observation and assessment of phase states of ambient and lab-generated sub-micron particles upon humidification. *RSC Adv.* **2021**, *11*, 15264−15272.
(88) Ault, A. P.; Moffet, R. C.; Baltrusaitis, J.; Collins, D. B.; Ruppel, M. J.; Cuadra-Rodriguez, L. A.; Zhao, D.; Guasco, T. L.; Ebben, C. J.; Geiger, F. M.; Bertram, T. H.; Prather, K. A.; Grassian, V. H. Size-dependent changes in sea spray aerosol composition and properties with different seawater conditions. *Environ. Sci. Technol.* **2013**, *47*, 5603−5612.
(89) May, N. W.; Axson, J. L.; Watson, A.; Pratt, K. A.; Ault, A. P. Lake spray aerosol generation: a method for producing representative particles from freshwater wave breaking. *Atmos. Meas. Tech.* **2016**, *9*, 4311−4325.
(90) Ault, A. P.; Zhao, D.; Ebben, C. J.; Tauber, M. J.; Geiger, F. M.; Prather, K. A.; Grassian, V. H. Raman microspectroscopy and vibrational sum frequency generation spectroscopy as probes of the bulk and surface compositions of size-resolved sea spray aerosol particles. *Phys. Chem. Chem. Phys.* **2013**, *15*, 6206−6214.
(91) Venkateswarlu, P.; Bist, H.; Jain, Y. Laser excited Raman spectrum of ammonium sulfate single crystal. *J. Raman Spectrosc.* **1975**, *3*, 143−151.
(92) Vargas Jentzsch, P.; Kampe, B.; Ciobotă, V.; Rösch, P.; Popp, J. Inorganic salts in atmospheric particulate matter: Raman spectroscopy as an analytical tool. *Spectrochim. Acta, Part A* **2013**, *115*, 697−708.
(93) Doughty, D. C.; Hill, S. C. Raman spectra of atmospheric particles measured in Maryland, USA over 22.5 hrs using an automated aerosol Raman spectrometer. *J. Quant. Spectrosc. Radiat. Transfer* **2020**, *244*, No. 106839.
(94) Lei, Z.; Bliesner, S. E.; Mattson, C. N.; Cooke, M. E.; Olson, N. E.; Chibwe, K.; Albert, J. N. L.; Ault, A. P. Aerosol Acidity Sensing via Polymer Degradation. *Anal. Chem.* **2020**, *92*, 6502−6511.
(95) Rindelaub, J. D.; Craig, R. L.; Nandy, L.; Bondy, A. L.; Dutcher, C. S.; Shepson, P. B.; Ault, A. P. Direct Measurement of pH in Individual Particles via Raman Microspectroscopy and Variation in Acidity with Relative Humidity. *J. Phys. Chem. A* **2016**, *120*, 911−917.
(96) Ault, A. P.; Moffet, R. C.; Baltrusaitis, J.; Collins, D. B.; Ruppel, M. J.; Cuadra-Rodriguez, L. A.; Zhao, D.; Guasco, T. L.; Ebben, C. J.; Geiger, F. M.; Bertram, T. H.; Prather, K. A.; Grassian, V. H. Size-dependent changes in sea spray serosol composition and properties with different seawater conditions. *Environ. Sci. Technol.* **2013**, *47*, 5603−5612.
(97) Sobanska, S.; Hwang, H.; Choel, M.; Jung, H. J.; Eom, H. J.; Kim, H.; Barbillat, J.; Ro, C. U. Investigation of the Chemical Mixing State of Individual Asian Dust Particles by the Combined Use of Electron Probe X-ray Microanalysis and Raman Microspectrometry. *Anal. Chem.* **2012**, *84*, 3145−3154.
(98) Zhou, Q.; Pang, S. F.; Wang, Y.; Ma, J. B.; Zhang, Y. H. Confocal Raman Studies of the Evolution of the Physical State of Mixed Phthalic Acid/Ammonium Sulfate Aerosol Droplets and the Effect of Substrates. *J. Phys. Chem. B* **2014**, *118*, 6198−6205.
(99) Eddingsaas, N. C.; VanderVelde, D. G.; Wennberg, P. O. Kinetics and Products of the Acid-Catalyzed Ring-Opening of Atmospherically Relevant Butyl Epoxy Alcohols. *J. Phys. Chem. A* **2010**, *114*, 8106−8113.
(100) Piletic, I. R.; Edney, E. O.; Bartolotti, L. J. A computational study of acid catalyzed aerosol reactions of atmospherically relevant epoxides. *Phys. Chem. Chem. Phys.* **2013**, *15*, 18065−18076.
(101) Lei, Z. Y.; Olson, N. E.; Zhang, Y.; Chen, Y. Z.; Lambe, A. T.; Zhang, J.; White, N. J.; Atkin, J. M.; Holl, M. M. B.; Zhang, Z. F.; Gold, A.; Surratt, J. D.; Ault, A. P. Morphology and Viscosity Changes after Reactive Uptake of Isoprene Epoxydiols in Submicrometer Phase Separated Particles with Secondary Organic Aerosol Formed from Different Volatile Organic Compounds. *ACS Earth Space Chem.* **2022**, *6*, 871−882.
(102) Bauer, S. E.; Ault, A.; Prather, K. A. Evaluation of aerosol mixing state classes in the GISS modelE-MATRIX climate model using single-particle mass spectrometry measurements. *J. Geophys. Res.: Atmos.* **2013**, *118*, 9834−9844.
(103) Fitzgerald, E.; Ault, A. P.; Zauscher, M. D.; Mayol-Bracero, O. L.; Prather, K. A. Comparison of the mixing state of long-range transported Asian and African mineral dust. *Atmos. Environ.* **2015**, *115*, 19−25.
(104) Bondy, A. L.; Bonanno, D.; Moffet, R. C.; Wang, B.; Laskin, A.; Ault, A. P. The diverse chemical mixing state of aerosol particles in the southeastern United States. *Atmos. Chem. Phys.* **2018**, *18*, 12595−12612.
(105) Craig, R. L.; Peterson, P. K.; Nandy, L.; Lei, Z.; Hossain, M. A.; Camarena, S.; Dodson, R. A.; Cook, R. D.; Dutcher, C. S.; Ault, A. P. Direct Determination of Aerosol pH: Size-Resolved Measurements of Submicrometer and Supermicrometer Aqueous Particles. *Anal. Chem.* **2018**, *90*, 11232−11239.
(106) Gunsch, M. J.; May, N. W.; Wen, M.; Bottenus, C. L. H.; Gardner, D. J.; VanReken, T. M.; Bertman, S. B.; Hopke, P. K.; Ault, A. P.; Pratt, K. A. Ubiquitous influence of wildfire emissions and secondary organic aerosol on summertime atmospheric aerosol in the forested Great Lakes region. *Atmos. Chem. Phys.* **2018**, *18*, 3701−3715.
(107) Gunsch, M. J.; Schmidt, S. A.; Gardner, D. J.; Bondy, A. L.; May, N. W.; Bertman, S. B.; Pratt, K. A.; Ault, A. P. Particle growth in an isoprene-rich forest: Influences of urban, wildfire, and biogenic air masses. *Atmos. Environ.* **2018**, *178*, 255−264.
(108) May, N. W.; Gunsch, M. J.; Olson, N. E.; Bondy, A. L.; Kirpes, R. M.; Bertman, S. B.; China, S.; Laskin, A.; Hopke, P. K.; Ault, A. P.; Pratt, K. A. Unexpected Contributions of Sea Spray and Lake Spray Aerosol to Inland Particulate Matter. *Environ. Sci. Technol. Lett.* **2018**, *5*, 405−412.
(109) Virtanen, A.; Joutsensaari, J.; Koop, T.; Kannosto, J.; Yli-Pirila, P.; Leskinen, J.; Makela, J. M.; Holopainen, J. K.; Poschl, U.; Kulmala, M.; Worsnop, D. R.; Laaksonen, A. An amorphous solid state of biogenic secondary organic aerosol particles. *Nature* **2010**, *467*, 824−827.
(110) Virtanen, A.; Kannosto, J.; Kuuluvainen, H.; Arffman, A.; Joutsensaari, J.; Saukko, E.; Hao, L.; Yli-Pirila, P.; Tiitta, P.; Holopainen, J. K.; Keskinen, J.; Worsnop, D. R.; Smith, J. N.; Laaksonen, A. Bounce behavior of freshly nucleated biogenic secondary organic aerosol particles. *Atmos. Chem. Phys.* **2011**, *11*, 8759−8766.

https://doi.org/10.1021/acs.est.2c01579
Environ. Sci. Technol. 2022, 56, 10596−10607